SINTEF
PROCEEDINGS
2

Proceedings of the 12th International Conference on Computational Fluid Dynamics in the Oil & Gas, Metallurgical and Process Industries

Progress in Applied CFD – CFD2017

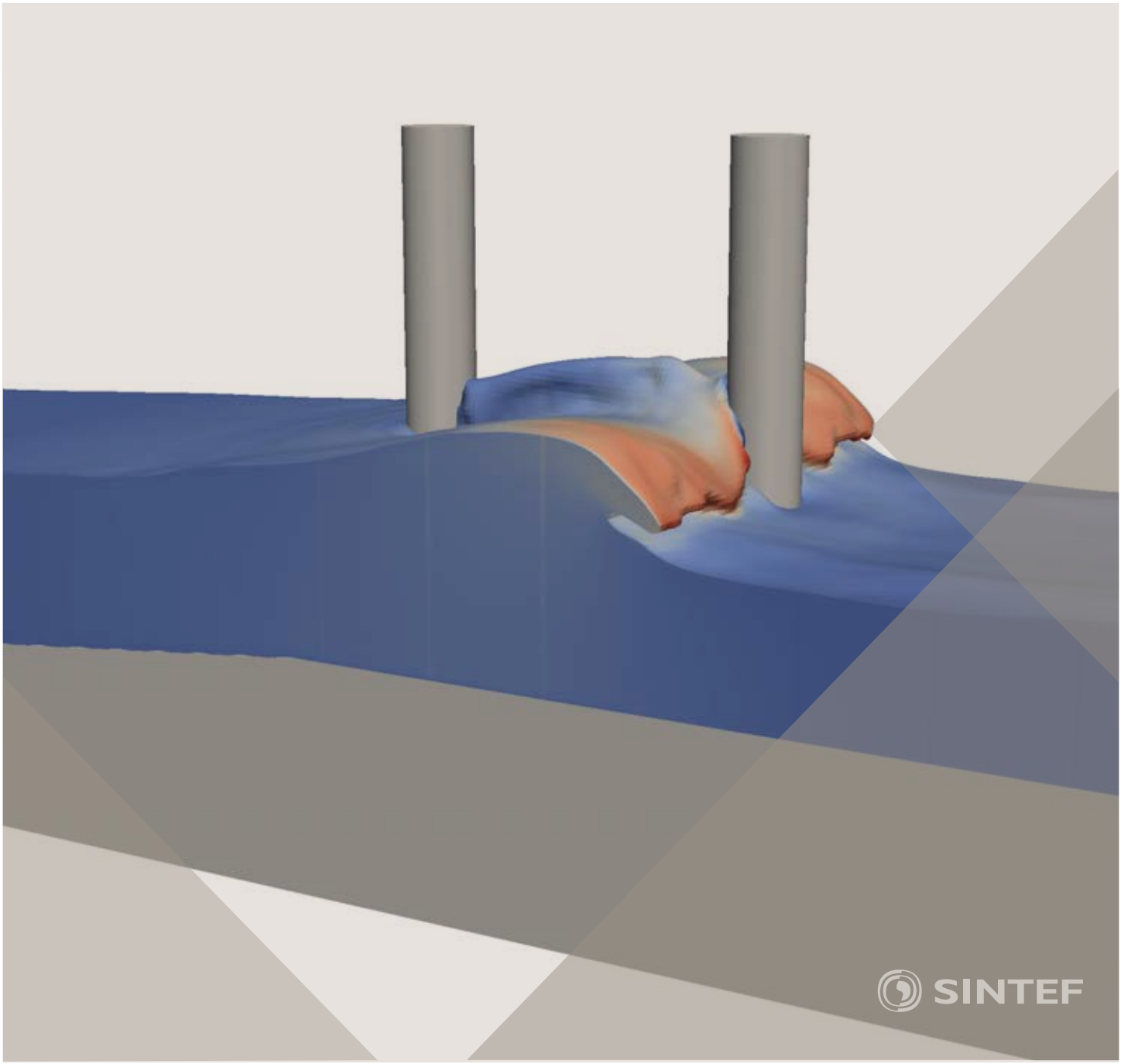

SINTEF Proceedings

Editors:
Jan Erik Olsen and Stein Tore Johansen

Progress in Applied CFD – CFD2017

Proceedings of the 12th International Conference on Computational Fluid Dynamics in the Oil & Gas, Metallurgical and Process Industries

SINTEF Academic Press

SINTEF Proceedings no 2
Editors: Jan Erik Olsen and Stein Tore Johansen
Progress in Applied CFD – CFD2017
Selected papers from 10th International Conference on Computational Fluid Dynamics in the Oil & Gas, Metallurgical and Process Industries

Key words:
CFD, Flow, Modelling

Cover, illustration: Arun Kamath

ISSN 2387-4295 (online)
ISBN 978-82-536-1544-8 (pdf)

SINTEF Academic Press
Address: Forskningsveien 3 B
PO Box 124 Blindern
N-0314 OSLO
Tel: +47 73 59 30 00
Fax: +47 22 96 55 08

www.sintef.no/byggforsk
www.sintefbok.no

SINTEF Proceedings
SINTEF Proceedings is a serial publication for peer-reviewed conference proceedings on a variety of scientific topics.
The processes of peer-reviewing of papers published in SINTEF Proceedings are administered by the conference organizers and proceedings editors. Detailed procedures will vary according to custom and practice in each scientific community.

PREFACE

This book contains all manuscripts approved by the reviewers and the organizing committee of the 12th International Conference on Computational Fluid Dynamics in the Oil & Gas, Metallurgical and Process Industries. The conference was hosted by SINTEF in Trondheim in May/June 2017 and is also known as CFD2017 for short. The conference series was initiated by CSIRO and Phil Schwarz in 1997. So far the conference has been alternating between CSIRO in Melbourne and SINTEF in Trondheim. The conferences focuses on the application of CFD in the oil and gas industries, metal production, mineral processing, power generation, chemicals and other process industries. In addition pragmatic modelling concepts and bio-mechanical applications have become an important part of the conference. The papers in this book demonstrate the current progress in applied CFD.

The conference papers undergo a review process involving two experts. Only papers accepted by the reviewers are included in the proceedings. 108 contributions were presented at the conference together with six keynote presentations. A majority of these contributions are presented by their manuscript in this collection (a few were granted to present without an accompanying manuscript).

The organizing committee would like to thank everyone who has helped with review of manuscripts, all those who helped to promote the conference and all authors who have submitted scientific contributions. We are also grateful for the support from the conference sponsors: ANSYS, SFI Metal Production and NanoSim.

Stein Tore Johansen & Jan Erik Olsen

Organizing committee:

Conference chairman: Prof. Stein Tore Johansen
Conference coordinator: Dr. Jan Erik Olsen
Dr. Bernhard Müller
Dr.Sigrid Karstad Dahl
Dr.Shahriar Amini
Dr.Ernst Meese
Dr.Josip Zoric
Dr.Jannike Solsvik
Dr.Peter Witt

Scientific committee:

Stein Tore Johansen, SINTEF/NTNU
Bernhard Müller, NTNU
Phil Schwarz, CSIRO
Akio Tomiyama, Kobe University
Hans Kuipers, Eindhoven University of Technology
Jinghai Li, Chinese Academy of Science
Markus Braun, Ansys
Simon Lo, CD-adapco
Patrick Segers, Universiteit Gent
Jiyuan Tu, RMIT
Jos Derksen, University of Aberdeen
Dmitry Eskin, Schlumberger-Doll Research
Pär Jönsson, KTH
Stefan Pirker, Johannes Kepler University
Josip Zoric, SINTEF

CONTENTS

INVESTIGATING THE NUMERICAL PARAMETER SPACE FOR A STENOSED PATIENT-SPECIFIC INTERNAL CAROTID ARTERY MODEL

Viviana MANCINI[1] & Aslak BERGERSEN[2], Patrick SEGERS[1], Kristian VALEN-SENDSTAD[2*]

[1] Ghent University, IBiTech-bioMMeda, 9000 Ghent, BELGIUM

[2] Simula Research Laboratory, Computational Cardiac Modelling, 1325 Lysaker, NORWAY

* E-mail: kvs@simula.com

ABSTRACT

Systemic risk factors are known to correlate with cardiovascular diseases, but e.g., atherosclerotic plaques are focally distributed and highlight the role of hemodynamically induced forces on vascular remodeling. Computational fluid dynamics (CFD) shows great promise for revealing mechanisms of atherosclerotic plaque progression, but the utility of CFD depends on the robustness of the numerical methods. The aim of the study was to investigate the parameter space of the numerical solutions to understand the resulting flow effects in a stenosed patient-specific internal carotid artery model. Simulations were performed on meshes consisting of 2 to 50M-elements meshes with a kinetic energy-preserving and minimally-dissipative solver, and time step size ranging from $1 \cdot 10^{-4}$ to $5 \cdot 10^{-6}$ seconds. The spatial refinement study revealed large differences in the instantaneous velocity fields, and the coarsest simulation did not provide any meaningful insight into the flow. That being said, the time-averaged results were in acceptable agreement for all spatial and temporal refinement levels. The variations in temporal resolution had minor effects, and the coarsest resolution was found to suffice. In conclusion, even for a highly accurate solver, a relatively high spatial resolution was needed to sufficiently resolve the flow, and we found the 22M-element mesh to offer an optimal balance between computational cost and time-averaged quantities.

Keywords: Stenosis, Computational Fluid Dynamics, Turbulence, Atherosclerotic plaque, Direct Numerical Simulation.

NOMENCLATURE

Latin Symbols

M	Million, [-]
PSD	Power spectral density, [m^2/s].
TKE	Turbulent kinetic energy, [m^2/s^2]
$\boldsymbol{u}(\boldsymbol{x}, t)$	Instantaneous velocity, [m/s].

Greek Symbols

ν	Kinematic viscosity, [m^2/s].
Δt	Time steps size, [s].
τ	Kolmogorov time scale, [s].
Δx	Mesh node spacing, [m].
η	Kolmogorov length scale, [m]
ε	Dissipation rate of TKE, [m^2/s^3]

Sub/superscripts

$\overline{\boldsymbol{u}}$	Mean velocity component, [m/s].
$\boldsymbol{u}'$	Fluctuating velocity component, [m/s].
$\lvert\boldsymbol{u}'\rvert$	Magnitude of $\boldsymbol{u}'$, [m/s]

INTRODUCTION

Atherosclerotic plaque is a leading cause of death in the western world, and causes a local narrowing of the arterial lumen also known as stenosis. The stenosis severity may increase over time to the point where it completely obstructs the blood flow. It is also known that blood clots can form downstream of the stenoses or that unstable plaques can loosen; both of which can result in ischemic stroke or heart attacks.

Computational fluid dynamics (CFD) shows great potential for revealing mechanisms of atherosclerotic plaque progression, e.g., in the carotid bifurcation by modeling patient-specific local hemodynamic forces (Steinman, 2002). However, the efficacy of CFD depends on the robustness of the methods and ability of reproduce results. This has shown to be challenging, especially for transitional biomedical flows, as demonstrated by Steinmann *et al*. (2012) who reported a large variability of jet penetration and complexity of patient-specific internal carotid artery aneurysm. In particular, it is not uncommon in the biomechanics literature to see the use of first order accurate and stabilized numerical schemes, which are well known to

be far too dissipative (Roache *et al.*, 1986). Such schemes have been argued applicable because of the relatively low Reynolds numbers of cardiovascular flows (Stewart *et al.*, 2012), relative to the transition point for steady flow in an infinitely long pipe (Reynolds, 1883). However, we have previously argued that Reynolds experiments might not be the best point of reference and showed that the use of "black-box" CFD solvers using default settings may be misleading us about the nature of the flow in the cardiovascular system (Valen-Sendstad and Steinman, 2014).

The aim of the current study was to use a verified and validated solver for laminar, transitional, and turbulent flows to find an adequate (under-resolved) direct numerical simulation reference solution from a spatial and temporal refinement study, with respect to point of transition and resolution of the flow instabilities through rigorous analysis, but also to determine the required resolution from a pragmatic biomedical point of view.

MODEL DESCRIPTION

Medical images of a common carotid bifurcation with severe stenosis (82% by area) located in the ICA of a 75 years old man were obtained from computed tomography angiography. The medical image was segmented using 3D Slicer (Iannaccone *et al.,* 2014), to obtain a plausible model of the vasculature. The Vascular Modelling Toolkit (Piccinelli *et al.*, 2009) was used to create meshes with a local refinement in the stenotic- and downstream region, but a constant global refinement between each mesh, resulting in four meshes with mean cell length (Δx) of $3.19 \cdot 10^{-4}$, $2.14 \cdot 10^{-4}$, $1.38 \cdot 10^{-4}$, and $1.05 \cdot 10^{-4}$ m. The meshes consists of 2, 6, 22, and 50 million (M) linear tetrahedral cells, and is referred to as the 2, 6, 22, and 50M-element mesh, respectively.

Simulations were performed using the open-source finite element CFD solver *Oasis* (Mortensen and Valen-Sendstad, 2015), where special care was taken to ensure a kinetic energy-preserving and minimally-dissipative numerical solution. We used continuous Lagrange elements with polynomial degree one for both the velocity, and pressure. The fluid properties were set to mimic water, with kinematic viscosity of $\nu = 1 \cdot 10^{-6}$ m^2/s to allow for direct comparison with *in-vitro* experiments. The inlet flow rate was set to be peak systolic, 585.52 ml/min, which corresponds to a Reynolds number of 1550 at the inlet. This deliberate choice was made to enable rigorous assessment of the temporal and spatial resolution with respect to the smallest scales present in the flow, however at the cost of a physiological artificial flow condition. A parabolic velocity profile was prescribed as inlet condition and no-slip condition was set along the walls. Figure 1 shows a curve fit based on work from Groen *et al.* (2010) that measured the flow split between the common and internal carotid artery as a function of degree of stenosis using MRI in 33 patients. The shape of the curve shows that most of the flow resistance occurs in the micro-vasculature for stenosis severity less than 65%, whereas the pressure drop across the stenosis dominates the resistance above this threshold. Using this model, the flow split between the internal and external carotid artery was set as to 31.8% and 68.2%, respectively.

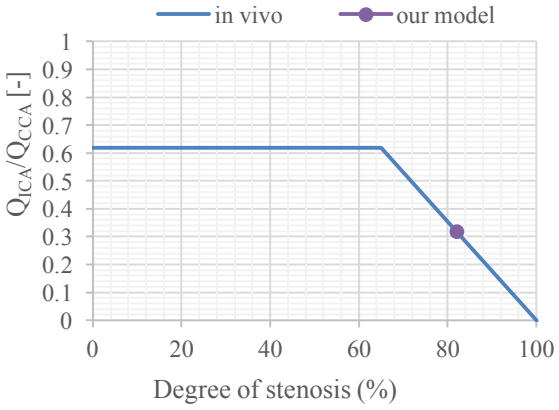

Figure 1: Outflow boundary conditions were set in order to match *in-vivo* values. The model is taken from the work of Groen et al. (2010) [10], who measured flow split as a function of degree of stenosis using MRI.

The flow was computed for 2 physical seconds on the coarsest mesh in order to cheaply washout initial transients associated with the artificial initial conditions. This simulation time was then the equivalent of 2 flow-throughs as the length of the model was 0.2 m, and the mean flow at the inlet was 0.1954 m/s. This flow field was then projected onto the 6, 22, and 50M-element meshes as initial conditions. To obtain a velocity field that was statistically converged, the mean velocities were based on simulations from 0.1 to 2.0 seconds. However, due to limitations on CPU hours, the 50M-element simulation was only simulated for 0.7 seconds, and the 22M-element simulation for 1.4 s.

We first performed a spatial refinement study at a fixed time step (Δt) of $2 \cdot 10^{-5}$ seconds. Using the least computationally expensive mesh that gave adequate results, a temporal refinement study was performed, with Δt ranging from $1 \cdot 10^{-4}$ to $5 \cdot 10^{-6}$ seconds.

Figure 2 shows the region of interest with four lines (A to D) and a point $\boldsymbol{P}$, located 1.7 cm (2.2 diameters) downstream of the center of the stenosis, where instantaneous velocity $\boldsymbol{u}(\boldsymbol{x}, t)$, was sampled. Reynolds decomposition was used to separate the instantaneous velocity from the time averaged, $\overline{\boldsymbol{u}}(\boldsymbol{x})$, and fluctuating, $\boldsymbol{u}'(\boldsymbol{x}, t)$, components, i.e., $\boldsymbol{u} = \overline{\boldsymbol{u}} + \boldsymbol{u}'$. Taking the fluctuating velocity magnitude signal, $|\boldsymbol{u}'|$, as input we computed the power spectral density (PSD) using Welch's method (Welch, 1967) with 32 segments, and a Hanning windowing function with 50 % overlap.

The coherent vortical structures were identified by the Q-criterion, which is a spatial region where the Euclidean norm of the vorticity tensor $\vec{\Omega}$ dominates the strain rate tensor $\vec{S}$ (Equation 1) (Hunt *et al.*, 1988).

$$Q = \frac{1}{2}\left[\left|\vec{\Omega}\right|^2 - \left|\vec{S}\right|^2\right] > 0$$

Equation 1: The comparison between the vorticity and strain rate tensors obtained through decomposition of the velocity gradient can be used as three-dimensional vortex identification criterion.

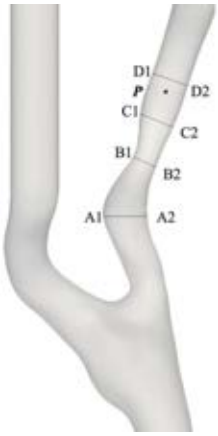

Figure 2: Region of interest of the model with lines A to D and point ***P***. Flow is going from bottom and up, or alternatively, the common carotid artery is branching into the external carotid (left), and internal carotid artery (right), respectively. The center of stenosis is defined as the midpoint of line B, and is based on the minimum area.

RESULTS

We first focus on basic flow features obtained on the 22M-element mesh shown in Figure 3, which depicts the volumetric velocity magnitude within the common carotid artery and ICA. The top of Figure 3 shows that the flow in the common artery is stable up until the carotid bifurcation, as the flow is uniform and there are no visible minor flow structures. At the bifurcation, the flow develops into a skewed profile towards the external wall of the ICA. Moreover, because of the pronounced curvature of the ICA the flow becomes unstable upstream of the stenosis, as observed in the left most bottom part of Figure 3. The stenosis causes the disturbed flow to accelerate into the stenosis, before the jet breaks down into an unstable flow downstream of the stenosis. However, the flow instabilities quickly dissipate further downstream, and the flow relaminarizes.

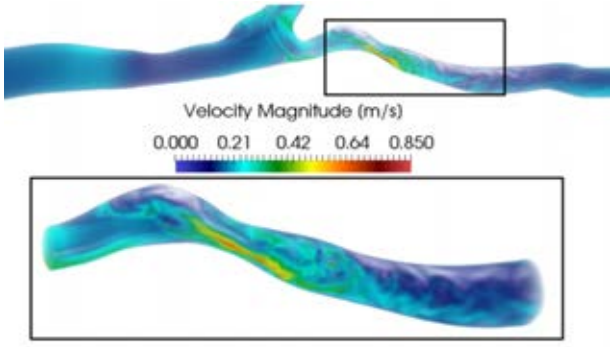

Figure 3: The top shows the volumetric rendering of the instantaneous velocity magnitude in the common and internal carotid arteries, and the bottom part is an enlargement of the box in the top part, showing the stenosis and downstream region.

Firstly, the Q-criterion was used to perform a quantitative comparison of the instantaneous velocity fields as shown in Figure 4. Moving from 2M through 50M there was a consistent increase in the number of vortices. In particular, upstream of the stenosis, the 22 and 50M-element simulations were phenotypically different from the 2 and 6M-element simulations, as there were smaller and more complex structures. In the downstream region in the 50M-element simulation the vortices were visually easier to see than in the 22M, however we can observe the same type and number of vortices. Visually there are large differences between mesh resolutions based on instantaneous flow fields. Moreover, the 2 and 6M-element simulations does not provide any physical insight into the flow.

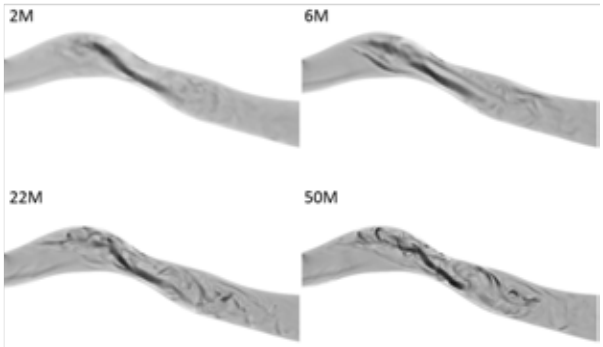

Figure 4: Volumetric rendering of coherent vortical structures at identical times within ICA identified by the Q-criterion.

To further assess the results from the spatial refinement study, we first consider the time-averaged velocities across the lines A to D, shown in Figure 5. In line A, upstream of the stenosis, we observe that the 2 and 6M-element simulations were similar, however relatively different from the 20 and 50M-element simulations which were phenotypically similar.

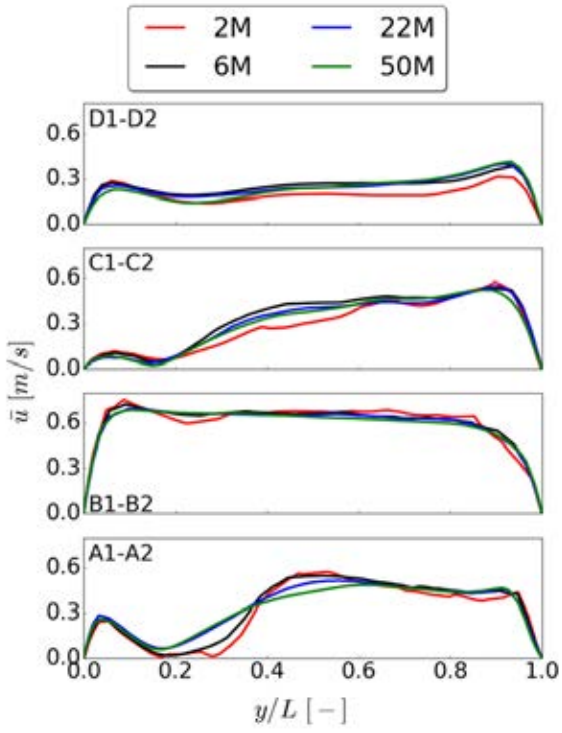

Figure 5: Time-averaged velocity along the four lines of interest for the spatial refinement study.

The time-averaged results were for all practical proposes equal at the stenosis (line B). In line C, when the jet from the stenosis breaks down the 22 and 50M-element simulations were similar, while the 2 and 6M-element simulations were under resolved, and under- and overestimated the centerline velocities, respectively. Finally, in line D at the end of the disturbed flow region, the 2M-element simulation under-estimates the time-

averaged velocity, while the other simulations were similar.

The PSD analysis of the fluctuating velocity signal at point ***P*** from Figure 2 is illustrated in Figure 6. The 2, 6, and 22M-element simulation seems to converge towards the 50M-element simulation. The 22 and 50M-element simulations were practically identical up until ~2000 Hz, however the spectra differs slightly at the higher frequencies. That being said, the analysis was admittedly based on different time-periods, and we would expect even better agreement if simulated for an equal period of time.

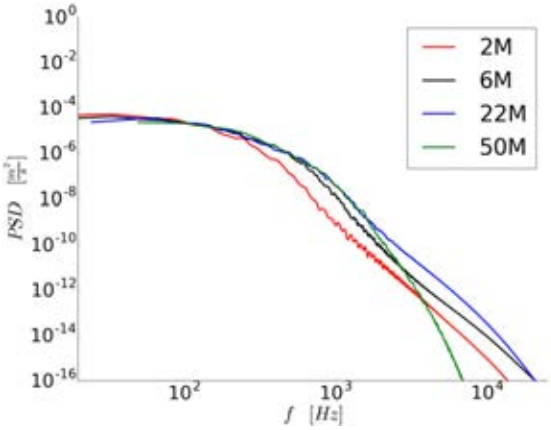

Figure 6: Power spectral density of the velocity field at point ***P*** from Figure 2, for the spatial refinement study.

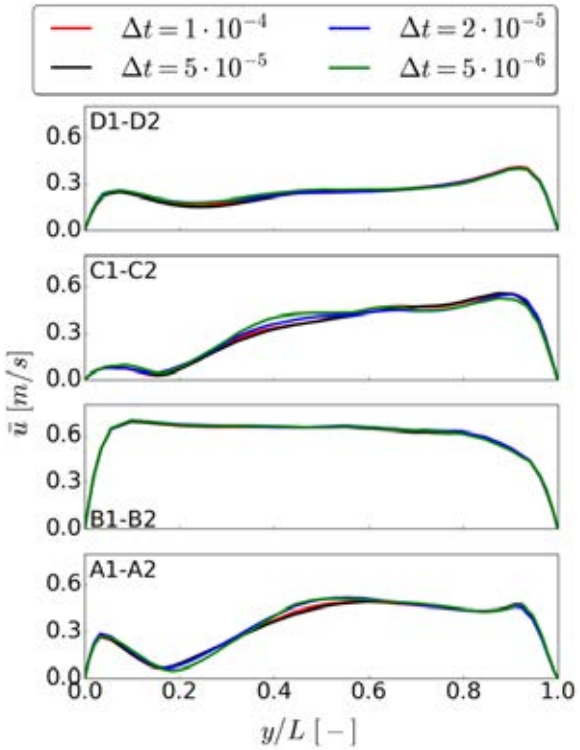

Figure 7: Time-averaged velocity along the four lines of interest for the spatial refinement study.

The temporal refinement study was evaluated similarly to the spatial refinement study. First, we considered the time-averaged velocity in the lines A to D, as shown in Figure 7. In all lines $1 \cdot 10^{-4}$, $5 \cdot 10^{-5}$, and $2 \cdot 10^{-5}$ were close to indistinguishable. In contrast, the $5 \cdot 10^{-6}$ simulation differed both in line A and C.

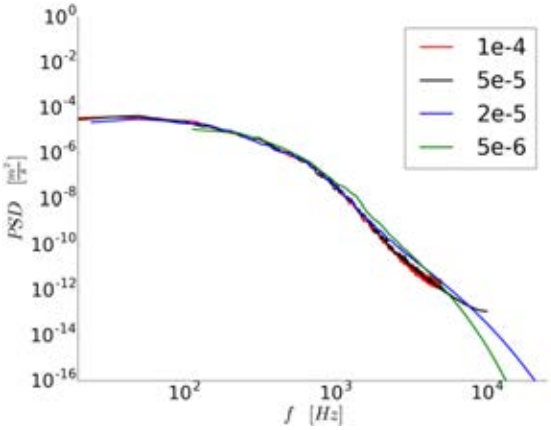

Figure 8: Power spectral density of the velocity field at point ***P*** from Figure 2, for the temporal refinement study.

The PSD analyses of the velocity traces recorded in point ***P*** are shown in Figure 8. We can observe that all of the different temporal simulations were from a pragmatic point of view equal. However, the temporally coarsest simulations naturally cannot capture the highest frequencies.

DISCUSSION

The aim of this study was to find an adequate (under-) resolved solution relative to the reference solution. From the spatial and temporal refinement study performed, a 22M-element mesh with a time step of $1 \cdot 10^{-4}$ seconds was found to be an optimal choice between computational cost and accuracy. This reference solution will be used in future studies on stenotic carotid bifurcations for comparison with turbulence modeling techniques. That being said, there is admittedly a minor difference between 22 and 50M-element meshes in Figure 5, in addition the simulations were not computed over the same number of physicals seconds. To assess if the 50M-element simulation was close enough to a proper direct numerical simulation we compared the spatial (Δx) and temporal (Δt) scales in the numerical simulation to the Kolmogorov length scale (η) and time scale (τ) (Kolmogorov, 1941), respectively, which can be calculated from the dissipation as shown in equation 2.

$$\eta = (\nu^3/\varepsilon)^{1/4}$$

$$\tau = (\nu/\varepsilon)^{1/2}$$

Equation 2: Kolmogorov scales depend on the kinematic viscosity (ν) and the rate of dissipation per unit mass of the turbulent kinetic energy (ε).

One of the assumptions behind the Kolmogorov hypothesis is that the turbulence is homogenous isotropic. It is obvious from Figure 3 that the (turbulent) kinetic energy is not homogenous. To assess whether the post-stenotic flow instabilities were isotropic, we computed the time-averaged mean squared fluctuating

velocities along the centerline between lines A and D in Figure 2. Figure 9 shows that the mean squared fluctuating velocities are at the same order of magnitude, however there are large variations, and thus cannot be called isotropic. Therefore, computing the Kolmogorov scales is a very conservative estimate of the smallest length scales in this mildly unstable flow.

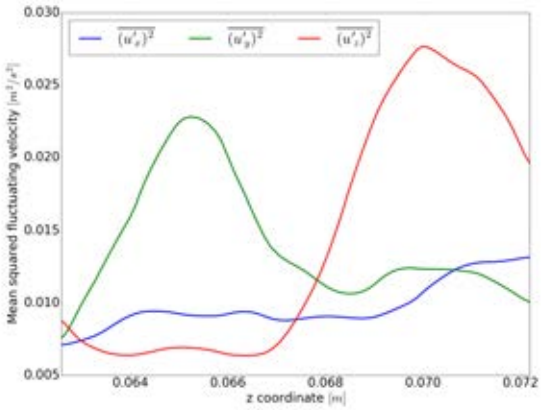

Figure 9: Mean squared fluctuating component of the velocity recorded along the centreline of the internal carotid artery.

The results of spatial assessment can be found in Table 1, displaying the characteristic node spacing Δx_{mean}, the smallest Kolmogorov length scale η_{min}, and the maximum ratio between Δx and η. There are two things to notice, first the Kolmogorov length scale converges, as the mesh is refined. Second, the maximum ratio between Δx and η on the two finest meshes are below 10, which is typically sufficient to capture > 95 % of the dissipation (Pope, 2001). If the simulations, from a numerical point of view, were truly converged, the ratio should be unity. However, the Kolmogorov scales only can be considered a conservative estimate as none of the rigid assumptions behind the hypothesis are met in this weakly unstable flow. Moreover, the differences between the 22, and 50M-element simulations were negligible, and a finer simulation will most likely not provide additional insight. We therefore consider the 50M-element simulation sufficiently refined from a pragmatic point of view, and by extension the 22M-element mesh for biomedical applications, where one is typically interested in a rapid classification once the tools are validated.

Furthermore, the difference in CPU hours is substantial, the 22M simulation with $\Delta t = 1 \cdot 10^{-4}$ seconds used 1420 CPU hours on 96 cores, while the 50M simulation $\Delta t = 2 \cdot 10^{-5}$ seconds would have spent 16 496 CPU hours on 128 cores to simulate 2 physical seconds, thus an order of magnitude difference.

Table 1: Comparison between Kolmogorov length scale $\boldsymbol{\eta}$ and the spatial scale of the numerical grid $\boldsymbol{\Delta x}$.

Number of cells	**2M**	**6M**	**22M**	**50M**
Δx_{mean}[m]	3.19E-4	2.14E-4	1.38E-4	1.05E-4
η_{min} [m]	9.81E-6	9.30E-6	8.91E-6	8.58E-6
$(\Delta x/\eta)_{max}$ [-]	21.93	14.04	9.31	7.49

The temporal assessment of the flow simulation can be found in Table 2, showing the minimum Kolmogorov time scale τ_{min} and the ratio between the numerical time scale Δt and τ_{min}. The two best resolved simulations were below the Kolmogorov time scale. However, we can observe from the PSD in Figure 8, that there was energy at higher fluctuations then the Nyquist frequency for the suggested Δt. If we are interested in the mean flow features, this cutoff is not important as there are for all practical purposes, no energy in the fluctuating component above 5000 Hz. However, since we are studying the fluctuations in the post-stenotic region, these high frequency fluctuations might be important. If such high frequency fluctuations were of interest, then the mesh itself might be the limiting factor, as the eddies associated with the high frequencies cannot be represented in mesh.

All quantitative analyses shown here were based on time-averaged results. However, there are evidences from the biomedical literature that temporal changes might be play an important role in remodeling of the arteries (Valen-Sendstad *et al.,* 2011, 2013, 2014).

From a numerical point of view, an even larger time step might have been acceptable, but $\Delta t = 1 \cdot 10^{-4}$ seconds is very close to the stability criteria of the numerical scheme used in the solver. The Courant–Friedrichs–Lewy (CFL) number for the 22M-element mesh simulation was 1.3, and the typical limit for this solver is 3-4 CFL.

Table 2: Comparison between Kolmogorov time scale $\boldsymbol{\tau}$ and the temporal scale of the simulations $\boldsymbol{\Delta t}$.

$\boldsymbol{\Delta t}$ **[s]**	**1.00E-4**	**5.00E-5**	**2.00E-5**	**5.00E-6**
τ_{min} [s]	7.96E-5	7.96E-5	7.93E-5	7.92E-5
$\Delta t/\tau_{min}$ [-]	1.2563	0.6281	0.2522	0.0631

We have admittedly not tested all parameters of the complete solution strategy space, exemplified by numerical schemes, viscosity models, compliant walls, etc.

A limitation of the current study is first of all that the simulations were not run for the same period of time. Secondly, the simulations were performed assuming rigid walls. However, compliant effects are normally considered negligible, and is nevertheless not of any importance in arterial growth and remodeling (Malek *et al.,* 1999). That being said, the effect of a compliant model in combination with turbulent-like flows remains to be assessed. Furthermore, the fluid used for these simulations was water instead of blood to allow for direct comparison against *in-vitro* experiments, which will be the focus of future work. However, non-Newtonian effects have shown to have negligible effects on the hemodynamics of carotid bifurcations and intracranial aneurysms (Lee and Steinman, 2007; Khan *et al.*, 2016).

As part of a larger consortium, the final aim of this line of investigation is to build a non-contact device to diagnose severe stenosis in the carotid arteries through the analysis of neck's skin displacement. We will therefore compute the sensitivity of the flow split and of noise in the inflow pulse through in-silico experiments,

since both factors can be challenging to control in the in-vitro experiments.

CONCLUSION

We analyzed the flow field of a patient-specific carotid artery bifurcation with severe stenosis. The flow was found to become unstable already upstream of the stenosis because of flow separation at the bifurcation. The acceleration and deceleration of the flow caused by the stenosis itself led to the occurrence of vortices which propagated downstream of the stenosis until relaminarization started around 4 cm downstream.

We found an adequate under-resolved solution relative to the reference solution. From the spatial and temporal refinement study performed, a 22M mesh with a time step of $\Delta t = 1 \cdot 10^{-4}$ seconds was found to be an optimal choice between computational cost and accuracy.

REFERENCES

GROEN, H.C., SIMONS, L., VAN DEN BOUWHUIJSEN, Q.J., BOSBOOM, E.M.H., GIJSEN, F.J., VAN DER GIESSEN, A.G., VAN DE VOSSE, F.N., HOFMAN, A., VAN DER STEEN, A.F., WITTEMAN, J.C. *et al.* (2010). "MRI-based quantification of outflow boundary conditions for computational fluid dynamics of stenosed human carotid arteries". *Journal of Biomechanics*, **43(12)**, 2332–2338.

HUNT, J.C., WRAY, A.A. and MOIN, P. (1988). "Eddies, streams, and convergence zones in turbulent flows". *Center for Turbulence Research,* **Report CTR-S88**.

IANNACCONE, F., DE BOCK, S., DE BEULE, M., VERMASSEN, F., VAN HERZEELE, I., VERDONCK, P., SEGERS, P. and VERHEGGHE, B. (2014). "Feasibility of a priori numerical assessment of plaque scaffolding after carotid artery stenting in clinical routine: proof of concept." *The International Journal of Artificial Organs*, **37(12)**, 928–939.

KHAN, M., STEINMAN, D. and VALEN-SENDSTAD, K. (2016). "Non-Newtonian versus numerical rheology: Practical impact of shear-thinning on the prediction of stable and unstable flows in intracranial aneurysms". *International Journal for Numerical Methods in Biomedical Engineering*.

KOLMOGOROV, A.N. (1941). "The local structure of turbulence in incompressible viscous fluid for very large Reynolds numbers". *Dokl. Akad. Nauk SSSR*, **30**, 301– 305.

LEE, S.W. and STEINMAN, D.A. (2007). "On the relative importance of rheology for image-based CFD models of the carotid bifurcation". *Journal of Biomechanical Engineering*, **129(2)**, 273–278.

MALEK, A.M., ALPER, S.L. and IZUMO, S. (1999). "Hemodynamic shear stress and its role in atherosclerosis". *JAMA*, **282(21)**, 2035–2042.

MORTENSEN, M. and VALEN-SENDSTAD, K. (2015). "Oasis: A high-level/high-performance open source Navier–Stokes solver". *Computer Physics Communications*, **188**, 177–188.

PICCINELLI, M., VENEZIANI, A., STEINMAN, D.A., REMUZZI, A. and ANTIGA, L. (2009). "A framework for geometric analysis of vascular structures: application to cerebral aneurysms". *IEEE Transactions on Medical Imaging*, **28(8)**, 1141–1155.

POPE, S.B. (2001). Turbulent flows. *IOP Publishing*.

REYNOLDS, O. (1883). "An experimental investigation of the circumstances which determine whether the motion of water shall be direct or sinuous, and of the law of resistance in parallel channels." *Proceedings of the Royal Society of London*, **35(224-226)**, 84–99.

ROACHE, P.J., GHIA, K.N. and WHITE, F.M. (1986). "Editorial policy statement on the control of numerical accuracy". *Journal of Fluids Engineering*, **108(1)**, 2–2.

STEINMAN, D.A. (2002). "Image-based computational fluid dynamics modeling in realistic arterial geometries". *Annals of Biomedical Engineering*, **30(4)**, 483–497.

STEINMAN, D.A., HOI, Y., FAHY, P., MORRIS, L., WALSH, M.T., ARISTOKLEOUS, N., ANAYIOTOS, A.S., PAPAHARILAOU, Y., ARZANI, A., SHADDEN, S.C. *et al.* (2013). "Variability of computational fluid dynamics solutions for pressure and flow in a giant aneurysm: the ASME 2012 summer bioengineering conference CFD challenge". *Journal of Biomechanical Engineering*, **135(2)**, 021016.

STEWART, S.F., PATERSON, E.G., BURGREEN, G.W., HARIHARAN, P., GIARRA, M., REDDY, V., DAY, S.W., MANNING, K.B., DEUTSCH, S., BERMAN, M.R. *et al.* (2012). "Assessment of CFD performance in simulations of an idealized medical device: results of FDAs first computational interlaboratory study". *Cardiovascular Engineering and Technology*, **3(2)**, 139–160.

VALEN-SENDSTAD, K. and STEINMAN, D. (2014). "Mind the gap: impact of computational fluid dynamics solution strategy on prediction of intracranial aneurysm hemodynamics and rupture status indicators". *American Journal of Neuroradiology*, **35(3)**, 536–543.

VALEN-SENDSTAD, K., MARDAL, K.A., MORTENSEN, M., REIF, B.A.P. and LANGTANGEN, H.P. (2011). "Direct numerical simulation of transitional flow in a patient-specific intracranial aneurysm". *Journal of Biomechanics*, **44(16)**, 2826–2832.

VALEN-SENDSTAD, K., MARDAL, K.A. and STEINMAN, D.A. (2013). "High-resolution CFD detects high-frequency velocity fluctuations in bifurcation, but not sidewall, aneurysms". *Journal of Biomechanics*, **46(2)**, 402–407.

VALEN-SENDSTAD, K., PICCINELLI, M. and STEINMAN, D.A. (2014). "High-resolution computational fluid dynamics detects flow instabilities in the carotid siphon: Implications for aneurysm initiation and rupture?" *Journal of Biomechanics*, **47(12)**, 3210–3216.

WELCH, P. (1967). "The use of fast Fourier transform for the estimation of power spectra: a method based on time averaging over short, modified periodograms". *IEEE Transactions on Audio and Electroacoustics*, **15(2)**, 70–73.